Electron density in the magnetosphere

R. E. Denton,[1] J. D. Menietti,[2] J. Goldstein,[3] S. L. Young,[4] and R. R. Anderson[2]

Received 22 September 2003; revised 17 June 2004; accepted 2 August 2004; published 30 September 2004.

[1] Observations of the electron density n_e based on measurement of the upper hybrid resonance frequency by the Polar spacecraft Plasma Wave Instrument (PWI) are available for March 1996 to September 1997, during which time the Polar orbit sampled all MLT values three times. In a previous study, we modeled the electron density dependence along field lines as $n_e = n_{e0}(R_{max}/R)^{\alpha}$, where n_{e0} is the equatorial electron density, $R_{max} \approx LR_E$ is the maximum geocentric radius R to any point on the field line, and $\alpha = \alpha_{model} = 8.0 - 3.0 \log_{10} n_{e0} + 0.28(\log_{10} n_{e0})^2 - 0.43(R_{max}/R_E)$, for all categories of plasma (plasmasphere and plasmatrough). (In the formula for α_{model}, n_{e0} is expressed in cm^{-3}.) Here, we illustrate the field line dependence using several example events. We show that the plasmapause is much more evident on the large radius portion of the orbit and that at $R \sim 2\ R_E$ the electron density tends to level out at large R_{max} to a constant value $\sim$100 cm^{-3}. We also present an example of plasmaspheric plasma extending out to at least $L \sim 9$ on the dawnside during particularly calm geomagnetic conditions (as indicated by low Kp). Then we present the average equatorial profiles of n_{e0} versus R_{max} for plasmasphere and plasmatrough. Our average plasmasphere profile is found to have values intermediate between those based on the models of Carpenter and Anderson and Sheeley et al. The plasmatrough equatorial density n_{e0} scales with respect to R_{max} like $R_{max}^{-3.4}$, but in the region for which our plasmatrough data is most reliable ($L \leq 6$), it is well fit by the $R_{max}^{-4.0}$ scaling of Sheeley et al. or the $R_{max}^{-4.5}$ scaling of Carpenter and Anderson. We present a simple interpretation for the field line dependence of the density. For large n_{e0}, such as occurs in the plasmasphere, α is close to zero on average (implying that n_e is roughly constant along field lines). When n_{e0} decreases, so does n_e at $R = 2\ R_E$, but the value there does not decrease much below 100 cm^{-3}. (It is unclear if this value is an absolute lower density limit because most often the upper hybrid resonance emission disappears at $R \sim 2\ R_E$ because $f_p/f_{ce} < 1$, where $f_p \propto \sqrt{n_e}$ is the plasma frequency and f_{ce} is the electron cyclotron frequency.) Finally, we examined the dependence of α and the density at the equator and at $R \sim 2\ R_E$ on the average $\langle Kp \rangle$ (Kp averaged with a 3-day timescale). There is no clear dependence of the average $\alpha - \alpha_{model}$ on $\langle Kp \rangle$ or on MLT. In the plasmasphere, n_{e0} decreases with respect to increasing $\langle Kp \rangle$. *INDEX TERMS:* 2768 Magnetospheric Physics: Plasmasphere; 2730 Magnetospheric Physics: Magnetosphere—inner; 2740 Magnetospheric Physics: Magnetospheric configuration and dynamics; 2794 Magnetospheric Physics: Instruments and techniques; *KEYWORDS:* magnetospheric electron density, empirical density model, plasmasphere

Citation: Denton, R. E., J. D. Menietti, J. Goldstein, S. L. Young, and R. R. Anderson (2004), Electron density in the magnetosphere, *J. Geophys. Res.*, *109*, A09215, doi:10.1029/2003JA010245.

1. Introduction

[2] Modeling the electron density n_e is important because n_e can serve as a proxy for the mass density ρ, which affects the timescale of the magnetospheric response to solar wind perturbations and determines the properties of ULF waves. More directly, the electron density can affect whistler waves that scatter radiation belt electrons and can affect radio communications at ionospheric altitudes.

[3] The seminal work on the distribution of the equatorial electron density n_{e0} is that of *Carpenter and Anderson* [1992]. More recently, models for n_{e0} have been developed by *Gallagher et al.* [2000] and *Sheeley et al.* [2001]. The latitudinal density dependence along field lines is less well known. Methods used to infer the latitudinal dependence of n_e along magnetic field lines include in situ spacecraft observations and passive remote sensing with whistler waves. Another recent technique for determining the field

[1]Department of Physics and Astronomy, Dartmouth College, Hanover, New Hampshire, USA.
[2]Department of Physics and Astronomy, University of Iowa, Iowa City, Iowa, USA.
[3]Space Science Department, Southwest Research Institute, San Antonio, Texas, USA.
[4]Air Force Research Laboratory, Hanscom Air Force Base, Massachusetts, USA.

0148-0227/04/2003JA010245$09.00

line distribution of n_e is active remote sensing using radio waves [*Reinisch et al.*, 2001, 2004]. This technique has the advantage that instantaneous profiles of n_e along the magnetic field line can be obtained, but so far the technique has been limited to cases where the equatorial electron density n_{e0} is large (several hundred cm^{-3}). Ultra low frequency (ULF) toroidal Alfvén frequencies have been used to infer the field line dependence of ρ (see references by *Menk et al.* [1999] and *Denton et al.* [2001] and also work by *Denton et al.* [2004] and *Takahashi et al.* [2004]).

[4] Three previous studies have used the Polar spacecraft plasma wave data to infer the typical dependence of electron density n_e along field lines. *Denton et al.* [2002a] used a method which did not initially assume any particular functional form for the parallel dependence but then found they could fit their results to the power law form

$$n_e = n_{e0}(R_{max}/R)^{\alpha}, \quad (1)$$

where R_{max} is the maximum geocentric radius R to any point on the field line (= LR_E for a dipole field), and n_{e0} is the value of n_e at $R = R_{max}$. (For our data set, $R = R_{max}$ occurs at the position of minimum magnetic field B_0, which we call the magnetic equator.) For a dipole magnetic field, this form becomes $n_e = n_{e0}\ (\cos(\lambda))^{-2\alpha}$, which is quite similar to the form recently used by *Reinisch et al.* [2004] and *Huang et al.* [2004], $n_e = n_{e0}\ (\cos[(\pi/2)\ (\alpha\lambda/\lambda_{inv})])^{-\beta}$, where λ_{inv} is the invariant (Earth's surface) value of the latitude λ. While we do not wish to claim that equation (1) is the optimal functional form for describing parallel density dependence, for a one parameter fit (α) it appears to do quite well [*Denton et al.*, 2002a], especially considering the large spread in the parallel dependence of the data. *Denton et al.* [2002a] listed α at a number of R_{max} values, finding, for instance, $\alpha = 0.8 \pm 1.2$ at $R_{max} = 4.4\ R_E$ and $\alpha = 2.1 \pm 1.4$ at $R_{max} = 7\ R_E$. *Goldstein et al.* [2001], using a method similar to that of the present paper, found an average value of $\alpha = 0.37 \pm 0.8$ for their plasmasphere data ($n_e \geq 100$ cm^{-3}) and an average value of $\alpha = 1.7 \pm 1.1$ for the plasmatrough ($n_e < 100$ cm^{-3}; they discarded outlying points before computing the errors). *Denton et al.* [2002b] used a much larger data set than that of *Goldstein et al.* [2001]. They mapped the magnetic field from the spacecraft position at the time of each measurement to determine R_{max} more accurately. Then they modeled the statistical average of α as a function of the equatorial density n_{e0} and R_{max} to find a single formula for α for all types of plasma (plasmasphere and plasmatrough)

$$\alpha_{model} = \alpha_{n_{e0}} + \alpha_{R_{max}}$$

$$\alpha_{n_{e0}} = 6.0 - 3.0\log_{10} n_{e0} + 0.28(\log_{10} n_{e0})^2, \quad (2)$$

$$\alpha_{R_{max}} = 2.0 - 0.43(R_{max}/R_E),$$

for $2.5\ R_E \leq R_{max} \leq 8.5\ R_E$, $2\ R_E \leq R \leq R_{max}$, and $2 \leq n_{e0} \leq 1500$ cm^{-3}. The average error between the observed α values and α_{model}, $\sqrt{\langle(\alpha - \alpha_{model})^2\rangle} = 0.65$. *Denton et al.* [2002b] stated that there was no remaining dependence of the average α on MLT or Kp but did not demonstrate this result due to space limitations.

[5] Here, after reviewing the basic method of analysis (section 2), we discuss some example events (section 3). We then present a number of average quantities, such as the average R_{max}-dependent profiles of n_{e0}, n_e at $R \sim 2\ R_E$ and α (section 4). In section 5 we examine the dependence of α, n_{e0}, and n_e at $R \sim 2\ R_E$ on the average $\langle Kp \rangle$ (Kp averaged with a 3-day timescale). We summarize our findings in section 6.

2. Polar Electron Density Data and Method of Analysis

[6] The electron density values used in this paper are obtained using the Polar Plasma Wave Instrument (PWI) [*Gurnett et al.*, 1995]. The electron number density can be determined from noise emission which has an upper edge in frequency at the upper hybrid resonance (UHR) frequency [*Goldstein et al.*, 2001]. For each data point, a field line mapping program was used to map the spacecraft location to the position along the field line with maximum radius, R_{max}. A Tsyganenko magnetic field model was used [*Tsyganenko*, 1995] as described by *Denton et al.* [2002a]. In cases for which solar wind data were available (92% of the data), we used the Tsyganenko 1996 [*Tsyganenko*, 1995] magnetic field model coupled with the International Geomagnetic Reference Field (IGRF) inner magnetic field model [*IAGA Division V Working Group 8*, 1991]. Where the solar wind data were not available, we substituted the Tsyganenko 1989c model [*Tsyganenko*, 1989] for the outer field.

[7] Figure 1 shows the path of the Polar spacecraft on 3 February 1997, projected onto a meridional plane (the Z coordinate is the same as the SM coordinate, and X is the other meridional coordinate). Owing to the nature of the Polar orbit, the trajectory of the spacecraft crosses a particular R_{max} value (i.e., L shell) at two different points, such as "1" and "2" in the figure. At these points we can calculate (from equation (1))

$$\alpha = \frac{\log(n_{e2}/n_{e1})}{\log(R_1/R_2)}, \quad (3)$$

where the subscripts 1 and 2 indicate data on the inner and outer segments of the Polar trajectory. (Errors in this procedure are discussed by *Denton et al.* [2002b].)

3. Example Events

3.1. The 3 February 1997 Event With a Clear Plasmapause

[8] Figure 2a shows the electron density n_e as determined by the PWI on 3 February 1997, 1322–1453 UT [*Denton et al.*, 2002b]. In Figure 2a, n_e is plotted versus R_{max} for the outer (thin curve) and inner (bold curve) portions of the orbit. (In the example plots, the thicker curve corresponds to the high density portion of the orbit.) Values of the radius R for both portions are plotted in Figure 2b. The resolution of the PWI data points is $\sim$0.1 R_E, as described by *Denton et al.* [2002b]. While it is clear that there is some azimuthal or temporal dependence (the plasmapause position is not exactly the same for the large and small radius portions of the orbit), in this particular case that dependence appears to be small. Furthermore, the smooth variation of density on both portions of the orbit gives evidence that in this case there is not a great amount of structure in the azimuthal direction.

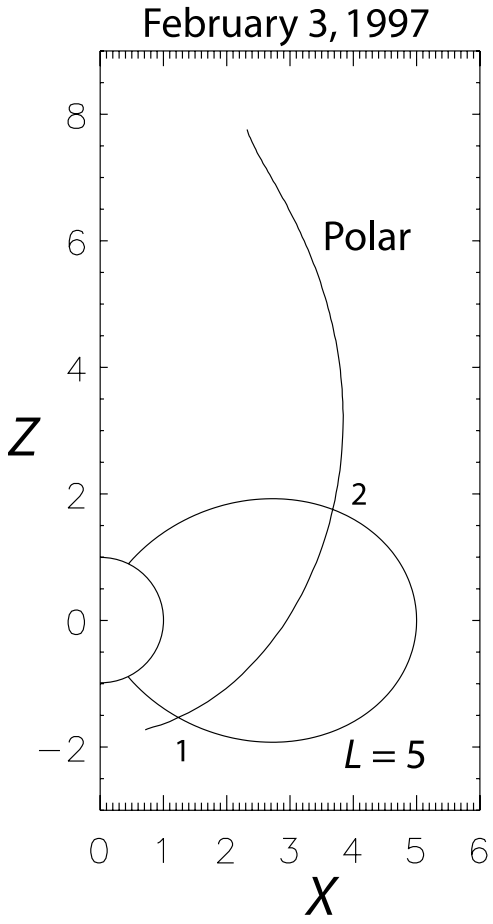

Figure 1. The path of the Polar spacecraft on 3 February 1997 projected onto a meridional plane. From the values of radius R and electron density n_e at points 1 and 2, equation (1) can be solved for α and n_{e0}.

[9] The α values plotted in Figure 2c are determined at a number of R_{max} values spaced approximately 0.1 R_E apart and within the range of R_{max} represented by the data on both inner and outer radius segments (here R_{max} = 3.0–6.0 R_E). Note that the value of α is small within the plasmasphere where the density on the inner and outer radius portions of the orbit are nearly the same. A value of $\alpha = 0$ corresponds to a flat, or constant, density dependence (equation (1)). For this particular event, α is also small just outside the plasmapause, but it increases farther out in the plasmatrough where the density on the inner and outer radius portions of the orbit differ.

[10] The variation of density along the field line can also be described in terms of a scale length. A physically meaningful definition of a scale length might be $L'_\alpha \equiv \sqrt{2n_{e0}/(d^2n_e/dl^2)}|_{l=0}$, where l is the length along the field line defined to be zero at the magnetic equator. Assuming $dn_e/dl|_{l=0} = 0$ at the magnetic equator (implied by equation (1)), L'_α is the distance along the field line from the equator at which the density is twice the equatorial value. In a dipole field, $L'_\alpha = (LR_E)/\sqrt{\alpha}$. Based on this fact, we define (for arbitrary magnetic field)

$$L_\alpha \equiv R_{max}/\sqrt{\alpha} \quad (4)$$

and plot values of L_α in Figure 2d. As was the case for α, values of L_α are not meaningful in the vicinity of the plasmapause where the gradients in n_e with respect to R_{max} are large. Outside the plasmapause ($R_{max} \gtrsim 3.6\ R_E$), L_α is roughly constant $\sim$4 R_E in this case.

[11] One notable feature of Figure 2a is that the density on the low radius portion of the orbit (thick curve corresponding to $R \sim 2\ R_E$) levels off at $\sim$100 cm^{-3} at large R_{max}. This is a common feature that we see in many Polar orbits and indicates that at large R_{max} the density is a stronger function of radius than of L shell. Values of $n_e \sim$ 100 cm^{-3} at $R \sim 2\ R_E$ with predominantly radial dependence are also found in the polar cap [*Persoon et al.*, 1983; *Gallagher et al.*, 2000; *Nsumei et al.*, 2003]. While at this altitude ($R \sim 2\ R_E$), the density at large R_{max} (but still on closed field lines) becomes more polar-cap-like, the density at the same R_{max} values but in the vicinity of the magnetic equator has different properties than the polar cap density. The differences are the R_{max} dependence (thin curve in Figure 2a), the fact that the radial dependence along the field lines is not so steep [*Denton et al.*, 2002b; *Nsumei et al.*, 2003], and the fact that n_{e0} decreases or is at least flat

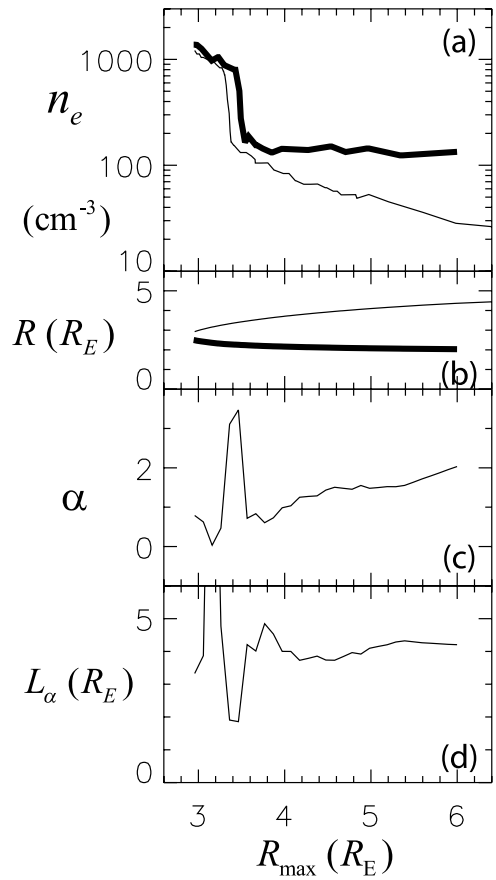

Figure 2. As a function of R_{max}, (a) the electron density n_e as determined from the PWI, (b) the Polar geocentric radius R, (c) the power law index α (equation (1)), and (d) the parallel scale length L_α (equation (4)) as determined from Polar data measured on 3 February 1997, 1322–1453 UT. In Figures 2a and 2b, the thin (bold) curve represents the profile of n_e determined at the large (small) radius portion of the orbit.

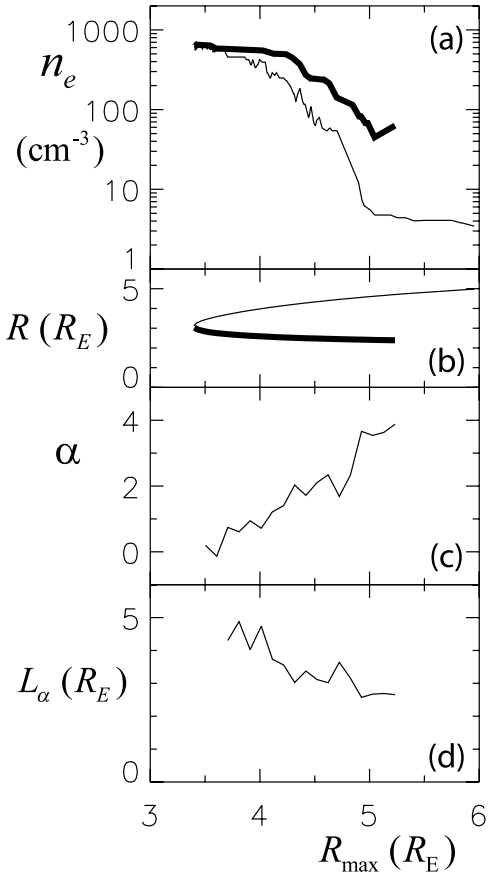

Figure 3. Same as Figure 2, except for data collected on 13 January 1997, 2140–2320 UT.

with respect to Kp (sections 5.2 and 5.3) rather than increasing with respect to Kp [*Nsumei et al.*, 2003]. All of these differences relate to trapping of particles in the plasmatrough and consequent buildup of n_{e0} on closed field lines. Even at $R \sim 2\ R_E$ the Kp dependence appears to be somewhat different as shown in section 5.2. The plasmatrough might then be considered a transition region sharing some properties of the polar cap and the plasmasphere.

3.2. Events for Which the Plasmapause Is Not So Apparent on the Low-Radius Portion of the Orbit

[12] Figure 3 shows an orbit with a plasmapause that is less steep. Though the inner and outer portions of the orbit have significantly different R (Figure 3b), the density structure on the two portions of the orbit is quite similar (Figure 3a). However, the density values for the inner curve (bold curve) do not drop to the low values of the outer curve (thin curve with $n_e \sim 4$ cm^{-3} at $R_{max} > 5\ R_E$). In this case, the density on the inner curve decreases to ~50 cm^{-3} at $R_{max} = 5.2\ R_E$. Correspondingly, the value of α is close to zero at low $R_{max} \lesssim 4\ R_E$ but is larger outside the plasmapause at $R_{max} \gtrsim 5\ R_E$.

[13] Figure 4 shows an orbit where the density just inside the plasmapause is not very far above 100 cm^{-3}. In this case, the plasmapause is evident on the high-radius portion of the trajectory (thin curve) but not on the low-radius portion of the trajectory (thick curve). Again, the density does not decrease very much below about 100 cm^{-3} for the low-radius portion of the orbit with $R \sim 2\ R_E$ (at least in the vicinity of the plasmapause at $R_{max} \sim 5.5\ R_E$; the behavior at the largest R_{max} values >7 R_E is not clear; see section 3.4). While n_e often levels off to ~100 cm^{-3} on the inner portion of the Polar orbit (with $R \sim 2\ R_E$) at large R_{max}, n_e can become quite large on the inner portion of the orbit at low R_{max} where the flux tubes are filled, that is, in the plasmasphere (Figures 2a, 3a, and 4a).

3.3. The 19 December 1996 Event With No Plasmapause

[14] Figure 5 shows data collected on 19 December 1996, 2154–2440 UT. This event falls in the "gradually decreasing" category of *Denton et al.* [2002b] (see Appendix A). The density gradually decreases on both inner and outer portions of the orbit so that no clear plasmapause is evident. Another possible interpretation of this data (as pointed out by a referee) is that the plasmapause is very wide, ending at $\sim R_{max} \sim 7\ R_E$. However, our opinion is that there is not much difference between a very wide plasmapause and no plasmapause at all. It is not clear how to distinguish a very wide plasmapause from the decrease in density with respect to R_{max} within the plasmasphere or plasmatrough. This event includes measurements out to $R_{max} = 9.8\ R_E$ based on the Tsyganenko 1996 magnetic field model [*Tsyganenko*, 1995] (out to $L = 8.7$ based on the dipole field model). The reason the spacecraft observes

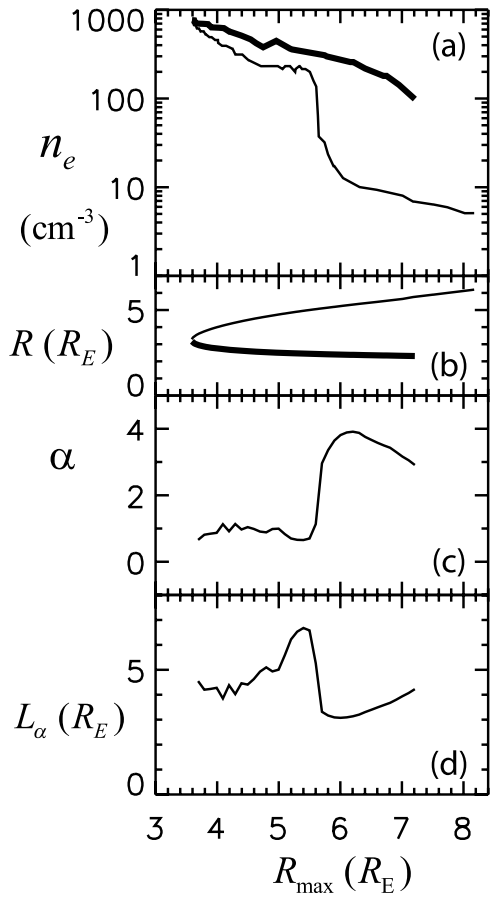

Figure 4. Same as Figure 2, except for data collected on 3 October 1996, 0401–0645 UT.

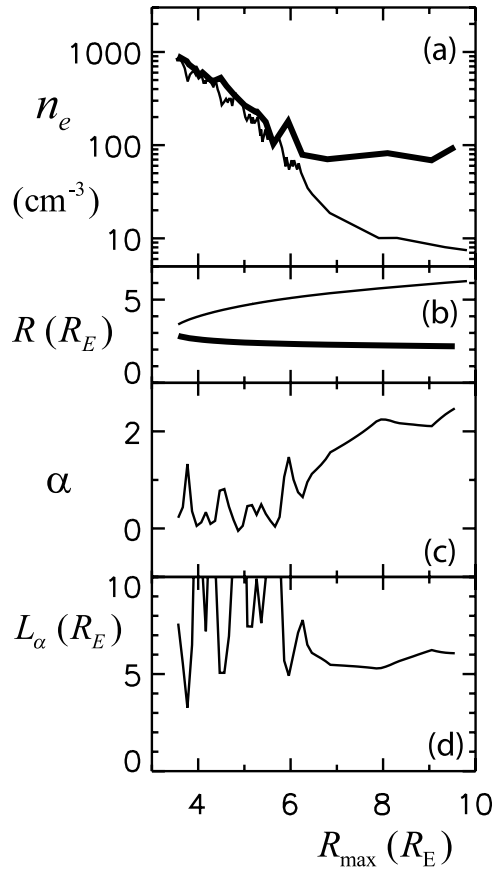

Figure 5. Same as Figure 2, except for data collected on 19 December 1996, 2154–2440 UT.

such large R_{max} values on the outer portion of the orbit is that in this case the magnetic latitude MLAT there is equal to 33.4°.

[15] It appears from Figure 5 that the plasmasphere, at least in the sense of the "gradually decreasing" plasma category (Appendix A), can extend out to large R_{max} (R_{max} ~ 9–10 R_E). Some observations of large density at large R_{max} correspond to plasma plumes [*Sandel et al.*, 2001], which usually occur on the duskside. However, the observation shown in Figure 5 occurred at magnetic local time MLT = 7 hours. Furthermore, similar profiles of density with respect to R_{max} were observed at the same MLT on the next two Polar passes and at dusk MLT ~20 hours, before and after the time corresponding to the event, as described in Appendix B. This extended plasmasphere occurred during an extended period of low geomagnetic activity as indicated by low Kp (see Appendix B), a condition which normally allows the plasmasphere to expand. It is possible that the large densities are confined to azimuthally localized structures [*Sandel et al.*, 2001]. On the other hand, the number of observations at different times and at different MLT values (Appendix B) may indicate that the plasma density has increased to plasmaspheric levels throughout the magnetosphere $R_{max} \leq$ 10 R_E. At the least, the high-density region (or regions) must fill a significant fraction of the magnetosphere. In any case, regardless of whether the observed density is azimuthally localized or not this example clearly shows that there are cases for which there is no clear plasmapause, at least along a radial cut, and in this sense the plasma at these large R_{max} values is plasmasphere-like.

3.4. Loss of Data at Large R_{max}

[16] One common feature we see in all the example events (Figures 2–5) is the cutoff of the data at large R_{max} on the low-radius portion of the orbit; in each case, the data on the large radius portion of the orbit (thin curves in Figures 2a, 3a, 4a, and 5a) continues to larger R_{max} values than the data on the low radius portion (thick curves in Figures 2a, 3a, 4a, and 5a). For instance, in Figure 2a, the data on the low-radius portion of the orbit (thick curve) ends at R_{max} = 6.0 R_E, whereas the data on the high-radius portion (thin curve) continues to beyond the highest R_{max} value plotted (R_{max} = 6.4 R_E). We have investigated this data cutoff for the four events. In each case, it occurs when $f_p/f_{ce} \sim 1$, where f_p is the plasma frequency $\propto\sqrt{n_e}$ and f_{ce} is the electron cyclotron frequency proportional to the magnetic field B. The existence of the upper hybrid noise band generally requires f_p/f_{ce} 1 [*Tataronis and Crawford*, 1970].

[17] In the case of Figure 2 at MLT ~15 hours, the data cutoff at low radius, R = 2.0 R_E, occurs at R_{max} = 6 R_E. The density could be lower outside this location (leading to lower $f_p/f_{ce} \propto \sqrt{n_e}$), or the reduction in f_p/f_{ce} could be due to the increasing $f_{ce} \propto B$. The particle data (Polar TIMAS) and wave properties (PWI) indicate that Polar continues to be in the plasmatrough for some distance outside of R_{max} = 6.0 R_E. We simply do not know what the density is during this time. At L = 9.6 (based on a dipole field), Polar enters the auroral region, as indicated by the sudden appearance of enhanced broadband electrostatic waves and electromagnetic auroral hiss associated with this regions [*Gurnett and Inan*, 1988; *Lin et al.*, 1984].

[18] In the case of Figure 3, at MLT ~5.6 hours, the disappearance of the upper hybrid emission at low radius, R = 2.4 R_E, occurs at R_{max} = 5.2 R_E. Again, we do not know what the density is at larger R_{max}. In this case, however, the disappearance of the upper hybrid emission coincides with entry into the auroral region or cusp, as noted by a sudden change in the plasma wave spectrum as described in the last paragraph.

[19] The data associated with Figure 4 is similar to that for Figure 2. The largest R_{max} value for which we have a density measurement is at R_{max} = 7.2 R_E (R = 2.3 R_E and MLT ~ 11 hours). There is a transition to auroral zone properties at $L \sim 11$ (based on a dipole field). There could be a region of the plasmatrough in between the two regions for which we cannot measure the density. However, unlike the case of Figure 2a, in Figure 4a the density is apparently decreasing at the time that $f_p/f_{ce} \sim 1$ and the upper hybrid emission disappears. Therefore the plasmatrough density may very well decrease below 100 cm^{-3}.

[20] In the case of Figure 5, corresponding to MLT = 7.5 hours, the low-radius data cutoff is at R_{max} = 9.6 R_E (at $R \sim$ 2.2). This case is like that of Figure 3. The disappearance of the upper hybrid emission coincides with entry into the auroral region as noted by a sudden change in the plasma wave spectrum.

[21] In summary, the low-radius data cutoff was apparently associated with a drop in f_p/f_{ce} below unity. For two out of four of the events, our low-radius data cutoff occurred

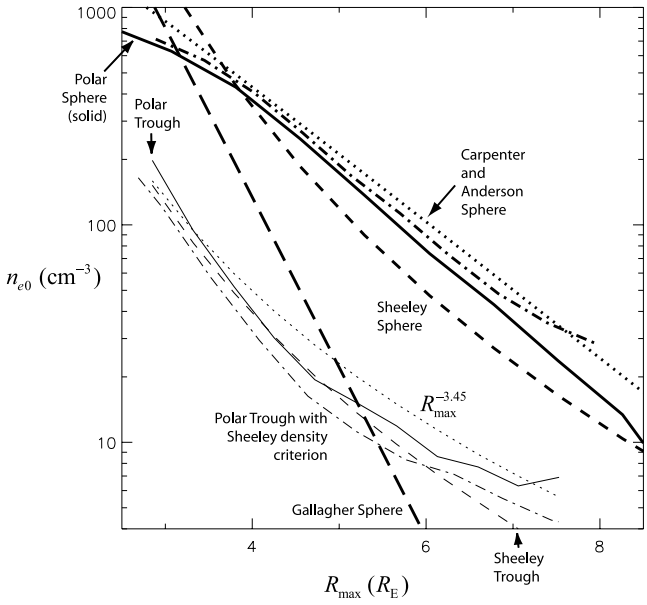

Figure 6. Equatorial electron density n_{e0} versus R_{max}. For the plasmasphere (thick curves), we plot the log average n_{e0} based on the Polar data (thick solid curve), the saturated plasmasphere model of *Carpenter and Anderson* [1992] (thick dotted curve), the plasmasphere model of *Sheeley et al.* [2001] (thick short dashed curve), and the plasmasphere model of *Gallagher et al.* [2000] (thick long dashed curve). For the plasmatrough (thin curves), we plot the log average n_{e0} based on the Polar data (thin solid curve), the best power law fit to our data (thin dotted curve), and the plasmatrough model of *Sheeley et al.* [2001] (thin dashed curve). The dot-dashed curves are the log average n_{e0} based on the Polar data but using the *Sheeley et al.* [2001] density criterion (equation (14)) to distinguish the data for the plasmasphere (thick dot-dashed curve) from the plasmatrough (thin dot-dashed curve).

in association with passage into the auroral zone. For the other two events, there may have been a region of the plasmatrough with decreased density outside of the region for which we were able to measure the density based on the presence of the upper hybrid resonance band. In one of these cases (Figure 4), the density appears to be dropping when the upper hybrid emission ceases. In the other case (Figure 2), there could be a decrease in density, or the change in f_p/f_{ce} could be explained by increasing B at low R.

4. R_{max} Dependence

4.1. R_{max} Dependence of n_{e0}

[22] Figure 6 shows the R_{max} dependence of the log average equatorial electron density n_{e0} for plasmasphere (thick solid curve) and the plasmatrough (thin solid curve). The categories of plasma were defined by visual inspection as described in Appendix A. For the purposes of this paper, the plasmasphere data set includes the "gradually decreasing" data set of *Denton et al.* [2002b] (see section 3.3 and Appendix A); the "gradually decreasing" plasma is assumed to be extended plasmasphere.

[23] The thick dotted curve in Figure 6 is *Carpenter and Anderson*'s [1992] saturated plasmasphere density

$$\log_{10}\left(n_{e0}/\mathrm{cm}^{-3}\right) = a_1 + a_2\bar{R}_{max} + (0.00127R_{Sun} - 0.0635)e^{-(\bar{R}_{max}-2)/1.5}, \quad (5)$$

where R_{Sun} is the average sunspot number $\sim$13 over the period of our data, we have averaged over their sinoidal local time dependence, Carpenter and Anderson's values for a_1 and a_2 are

$$a_1^{CA} = 3.90, \qquad a_2^{CA} = -0.315, \quad (6)$$

and we have substituted

$$\bar{R}_{max} = R_{max}/R_E \quad (7)$$

(= L for a dipole field) for their L. (The Carpenter and Anderson study used spacecraft data with MLAT < 30°, and the distinction between L based on a dipole field versus our $\bar{R}_{max}$ is likely to be less important than for our data set from the Polar spacecraft.) The short dashed curve in Figure 6 is the plasmasphere model of *Sheeley et al.* [2001]

$$n_{e0} = \left(1390\mathrm{cm}^{-3}\right)\left(3/\bar{R}_{max}\right)^{4.83}, \pm \left(440\mathrm{cm}^{-3}\right)\left(3/\bar{R}_{max}\right)^{3.60} \quad (8)$$

for $3 \le \bar{R}_{max} \le 7$.

[24] Our equatorial average plasmasphere n_{e0} values (thick solid curve) lie between the n_{e0} values of Carpenter and Anderson (thick dotted curve based on equation (5) with equation (6)) and those of Sheeley et al. (thick short-dashed curve based on equation (8)). Our plasmasphere data can be best fit using equation (5) with

$$a_1 = 3.78 \pm 0.18, \qquad a_2 = -0.324 \pm 0.038, \quad (9)$$

for $2.5 \le \bar{R}_{max} \le 8.0$. Our coefficients (equation (9)) agree with Carpenter and Anderson's values within the uncertainties. (The fact that the Polar n_{e0} values are lower than values from the other models at low $R_{max} \le 3.5\ R_E$ may be related to the boom oscillation problem on Polar [*Denton et al.*, 2002b].) On average, the Polar n_{e0} measurements are a factor of 1.9 off from our fit, equation (5) with equation (9) (varying in R_{max} bins from a factor of 1.4 off at $\bar{R}_{max} = 2.7$ to a factor of 2.0–2.5 off at $\bar{R}_{max} \ge 4.9$).

[25] The long dashed curve in Figure 6 is the plasmasphere model of *Gallagher et al.* [2000], which is equation (5) with a_1 and a_2 given by

$$a_1^{Gal} = 5.3, \qquad a_2^{Gal} = -0.79. \quad (10)$$

(Actually, Gallagher et al.'s equation for n_{e0} has extra terms other than equation (5), but equation (5) captures the main dependence of their model.) There is clearly a significant difference between the plasmasphere model of *Gallagher et*

al. [2000] and the other models. Gallagher et al.'s model (equation (5) with equation (10)) is based on ion particle data and might not have measured a significant fraction of the electron density at large R_{max}. On the other hand, the data used (DE-1 RIMS) was calibrated against measurements from the DE 1 Plasma Wave Instrument (D. Gallagher, private communication, 2004). Another possible explanation for the difference relates to the method by which the data was screened. Gallagher et al.'s data set is based on low Kp, with the 3-day weighted average (section 5.1) $\leq$1.3. They may have included data in their plasmaspheric data set that we would have classified as plasmatrough based on visual inspection (see Appendix A).

[26] As was already mentioned, the thin solid curve in Figure 6 is the log average plasmatrough density based on the Polar spacecraft data. *Carpenter and Anderson*'s [1992] plasmatrough model uses a power law form

$$n_{e0} = a_3(\bar{R}_{max})^{a_4}, \tag{11}$$

with $a_4 = -4.5$ and a_3 specified by a condition matching plasmasphere and plasmatrough density (we have substituted $\bar{R}_{max}$ for their L). Our plasmatrough data is best fit with $a_4 = -3.45$,

$$\log_{10}\left(n_{e0}/\mathrm{cm}^{-3}\right) = (3.77 \pm 0.31) + (-3.45 \pm 0.41)\log_{10}(\bar{R}_{max}), \tag{12}$$

fit for $2.9 \leq \bar{R}_{max} \leq 7.5$, and plotted as the thin dotted curve in Figure 6. On average, the Polar density measurements are a factor of 2.1 off from this model. *Sheeley et al.* [2001] found $a_4 = -4.0$. The value $a_4 = -4.0$ is what one would expect if the flux tube volume (per magnetic flux) $\propto L/B \sim R_{max}^4$ and the flux tube particle content (per magnetic flux) is constant across the plasmatrough (Appendix C). Their model for plasmatrough density is

$$n_{e0} = 124\ \mathrm{cm}^{-3}(3/\bar{R}_{max})^{4.0}, \pm 78\ \mathrm{cm}^{-3}(3/\bar{R}_{max})^{4.72}, \tag{13}$$

for $3 \leq \bar{R}_{max} \leq 7$, where we have averaged over their sinoidal local time dependence and have again substituted $\bar{R}_{max}$ for L. Their plasmatrough n_{e0} is plotted as the thin dashed curve in Figure 6. Our curve (thin solid curve) lies very close to that of Sheeley et al. (thin dashed curve) except at large R_{max} where our curve levels out to $\sim n_{e0} \sim 7\ \mathrm{cm}^{-3}$ (we will comment on this in the last paragraph of this subsection).

[27] *Sheeley et al.*'s [2001] study used plasma wave data as does ours (their data is found from observations by the CRRES spacecraft). One difference in Sheeley et al.'s data analysis is that they distinguished their plasmasphere and plasmatrough data using a criterion on density

$$n_{e0} = \left(10\ \mathrm{cm}^{-3}\right)(6.6/\bar{R}_{max})^4 \tag{14}$$

(correcting a misprint in their paper). Observations with density above (below) this value were assumed to be plasmasphere (plasmatrough). We separated plasmasphere and plasmatrough data for individual events using a more complicated procedure (Appendix A), similar to that of *Carpenter and Anderson* [1992]. To test whether the difference in results is due to this difference in method, we also separated plasmasphere and plasmatrough data (from all types of plasma) using the criterion in equation (14). The density values found using this method are plotted as dot-dashed curves in Figure 6. The thick dot-dashed curve (plasmasphere chosen with equation (14)) is close to and actually higher than the thick solid curve (our plasmasphere data set). Thus this difference in method cannot explain why the Sheeley et al. n_{e0} (thick short-dashed curve) is lower than ours (thick solid curve).

[28] The thin dot-dashed curve in Figure 6 (plasmatrough determined by equation (14)) is somewhat lower than our thin solid curve (log average for plasmatrough data set). The use of equation (14) to choose small densities results in a lower average density. This could help explain the difference in density values between the Sheeley et al. model (thin dashed curve) and our log average plasmatrough density (thin solid curve) at some values of R_{max}, such as $R_{max} > 5\ R_E$. On the other hand, the Polar PWI signal often drops out when the density is very low at large R_{max} (particularly when R is low; see section 3.4), and this may be the cause of the leveling out of our log average plasmatrough density to $\sim n_{e0} \sim 7\ \mathrm{cm}^{-3}$ at $R_{max} = 7$–$7.5\ R_E$. If we use our plasmatrough data only out to $R_{max} = 6.4\ R_E$, our best fit is

$$\log_{10}\left(n_{e0}/\mathrm{cm}^{-3}\right) = (4.13 \pm 0.46) + (-4.10 \pm 0.74)\log_{10}(\bar{R}_{max}), \tag{15}$$

and now the coefficient $a_4 = -4.10 \pm 0.74$ (see equation (11)) is equal to both the Sheeley et al. $a_4 = -4.0$ and Carpenter and Anderson $a_4 = -4.5$ values within the uncertainty.

4.2. R_{max} Dependence of Other Quantities

[29] In this subsection, we examine the R_{max} dependence of other quantities and explore the result of combining our field line density dependence model (equation (1) with equation (2)) with the R_{max}-dependent plasmasphere and plasmatrough n_{e0} profiles described in section 4.1 (solid curves in Figure 6). In Figure 7 a number of quantities are plotted versus R_{max}. The thick curves correspond to the plasmasphere, while the thin curves correspond to the plasmatrough. The solid curves result from an average. The solid curves in Figure 7a are the same log average n_{e0} values as were plotted in Figure 6. The solid curves in Figure 7b are the average α values. The dashed curves all relate to the log average values of n_e computed for $R = 2\ R_E$ (more precisely, for $1.8\ R_E \leq R \leq 2.2\ R_E$). The Polar spacecraft perigee was at $\sim R = 1.87$ (at the beginning of 1997), so $R = 2\ R_E$ is essentially the lowest radius sampled. The dashed curve in Figure 7a shows these log average values. The dashed curves in Figure 7b show the values of α found from equation (3) using the log average values of n_e from Figure 7a at the equator and at $R = 2\ R_E$ (solid and dashed curves from Figure 7a). The dotted curves all relate to the α_{model} model (equation (2)). The dotted curves in Figure 7b are the values of α_{model} with the log average n_{e0} values (solid curves in Figure 7a) as an input. The dotted curves in Figure 7a are the n_e values at $R = 2\ R_E$ based on these same α_{model} values (dotted curves in Figure 7b) and

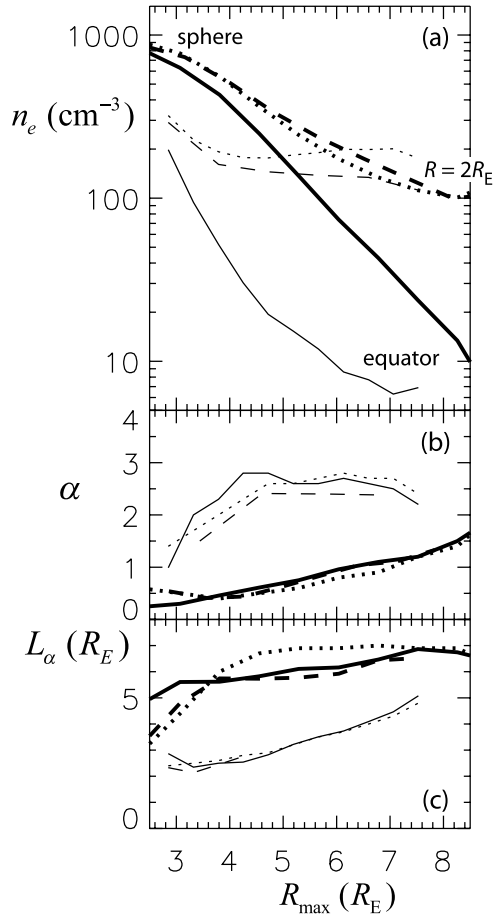

Figure 7. The R_{max} dependence of several quantities are plotted for the plasmasphere (thick curves) and plasmatrough (thin curves). In Figure 7a the solid curves are the log average equatorial electron density n_{e0}, the dashed curves are the log average values of n_e at $R = 2\ R_E$, and the dotted curves are the values of n_e at $R = 2\ R_E$ assuming the field line dependence (equation (1)) with $\alpha = \alpha_{model}$ (equation (2)) and using the log average n_{e0} (solid curve) as an input for n_{e0}. In Figure 7b the solid curves are the average α_{model} values, the dashed curves are the values of α found from equation (3) using the log average values of n_e from (a) at the equator and at $R = 2\ R_E$ (solid and dashed curves from (a)), and the dotted curves are the α_{model} values (equation (2)) as a function of the log average n_{e0} plotted in Figure 7a (solid curves in Figure 7a). In Figure 7c the curves are the values of the parallel scale length L_α found from equation (4) using the corresponding α values from Figure 7b.

the log average n_{e0} values (solid curves in Figure 7a). The parallel scale length values in Figure 7c are calculated from equation (4) using the corresponding α values plotted in Figure 7b. In other words, the thick solid curve in Figure 7c is the value of L_α based on the thick solid curve from Figure 7c, that is, the L_α value based on the average α for the plasmasphere.

[30] Figure 7b shows that the α values are relatively small, roughly 0–1, in the plasmasphere, while values around 2.5 are typical in the plasmatrough. Correspondingly, L_α is larger in the plasmasphere, $\sim$6 R_E for $4 \leq \bar{R}_{max} \leq 7$, as compared to the plasmatrough with $L_\alpha \sim 2.5$–5 R_E. (*Goldstein et al.* [2001] found $L_\alpha \sim 5.5\ R_E$ averaging over all types of plasma).

[31] As mentioned previously, the dotted curves in Figure 7a are the n_e values at $R = 2\ R_E$ using the α_{model} model with the log average n_{e0} values as an input. Both the curves for the plasmasphere (thick dotted curve) and plasmatrough (thin dotted curve) approach values close to 100 cm^{-3} at large R_{max}. Surprisingly, the plasmatrough curve levels off at somewhat higher density ($\sim$200 cm^{-3}) than the plasmasphere curve ($\sim$100 cm^{-3}). The log average values of n_e at $R_{max} = 2\ R_E$ also approach a value close to 100 cm^{-3} at large R_{max} (dashed curves in Figure 7a). However, in this case, the curve for the plasmasphere (thick dashed curve in Figure 7a) is everywhere higher than the curve for the plasmatrough (thin dashed curve in Figure 7a), as expected.

[32] The difference in the dotted and dashed curves in Figure 7a demonstrates the limitations of our model as expressed by equation (1) with equation (2). Seeing as the dotted curve in Figure 7a is the equatorial density extrapolated to $R = 2\ R_E$ and the dashed curve is the actual density at $R = 2\ R_E$, the fact that the dotted and dashed curves are almost the same for the plasmasphere data (thick curves) indicates that α_{model} (equation (2)) can be used to accurately extrapolate plasmaspheric equatorial densities down to $R = 2\ R_E$. On the other hand, for the plasmatrough (thin curves in Figure 7a), the difference between the thin dotted and dashed curves indicates a possible error on the order of a factor of 2 at the larger R_{max} values (5 R_E) when extrapolating equatorial densities to $R = 2\ R_E$. (It is not surprising that the agreement for the plasmasphere data is better considering that the plasmasphere α values are low so that the field line dependence is weak.) Correspondingly, the α values found three different ways and plotted in Figure 7b agree fairly well for the plasmasphere data, but for the plasmatrough, there is disagreement on the order of 0.5.

[33] Based on the observations described in section 3.4, we need to qualify our results. It is likely that sometimes n_e is lower than 100 cm^{-3} at low radius and large R_{max} and we are not able to measure the density because $f_p/f_{ce} < 1$ so that the upper hybrid noise band is not observed. This does lead to some doubt about our conclusion that the density at $R \sim 2$ R_E does not go significantly below 100 cm^{-3}. On the other hand, we often see the density level off to a value near 100 cm^{-3} when the equatorial density is still decreasing with respect to R_{max} (Figures 2a and 5a). Furthermore, if we were to add observations with significantly lower density at $R \sim 2\ R_E$, that would have the effect of lowering the α values calculated using the average density at the equator and at $R = 2\ R_E$ (dashed curve in Figure 7b). However, for the plasmatrough data (for which low density at $R \sim 2\ R_E$ is more likely), these values are already lower than the average α values based on all the measurements, including those at larger R (thin solid curve in Figure 7b).

4.3. Meridional Dependence

[34] Features of the field line dependence are shown in a different way in Figure 8. Here, we plot in a meridional plane contour lines for our plasmatrough density (equation (12) with equation (2)) for the field line dependence. The thin solid curves are the density contours, the thick solid curves

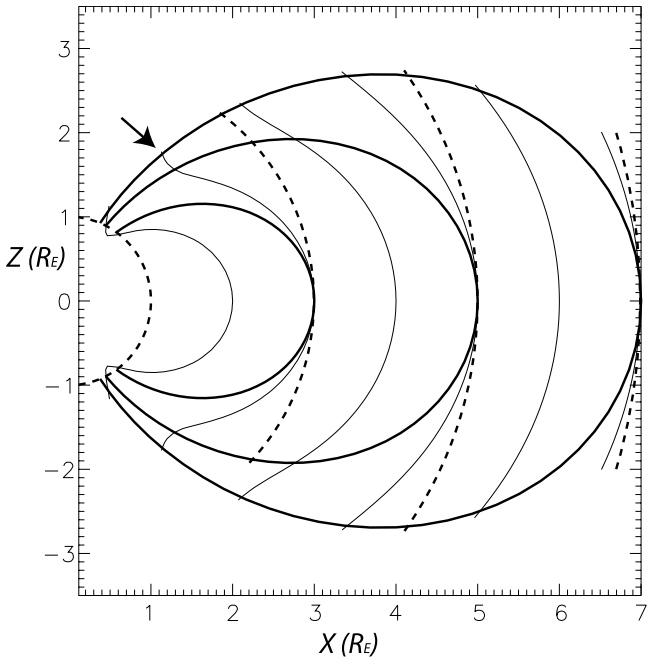

Figure 8. Meridional plane showing contour lines (thin solid curves) of the density given by equation (12) with equation (2) for the field line dependence. The thick solid curves are dipole field lines, and the thick dashed curves are circular.

are dipole field lines, and the thick dashed curves are circular (the curve at a radius of 1 R_E is the Earth's surface). Note that in the region close to the magnetic equator the density contour that crosses the magnetic equator at low $L = 3$ has a similar shape to the dipole field because α is small for the large density at this L (implying a flat density along magnetic field lines). On the other hand, the contour line that crosses the magnetic equator at larger $L = 7$ is more circular in shape (implying a density dependence that is closer to a function of radius). Note also that the contour line for $L = 3$ has nearly constant radius at $R \sim 2\ R_E$ (position of arrow). This feature corresponds to the leveling out of the density with respect to R_{max} at $R \sim 2\ R_E$ (Figure 7a).

4.4. Simple Model for α

[35] Equation (2) describes the field line variation of n_e (α) in terms of n_{e0} and R_{max}. The strongest dependence is on n_{e0} [*Denton et al.*, 2002b]. Our results might be summarized by two simple statements. For large n_{e0}, such as occurs in the plasmasphere, α is on average close to zero (implying that n_e is roughly constant along the field line). When n_{e0} decreases, so does n_e at $R = 2\ R_E$, but the value there does not decrease below $\sim$100 cm^{-3}. This is apparently because when flux tubes become depleted, the density at low radius $R \sim 2\ R_E$ is approximately just a function of R, independent of R_{max}. (Note that the field lines are converging at low altitude owing to the geometry of the dipole field.) Figure 9 shows a simple application of these ideas. The thick and thin solid, dashed, and dotted curves are the same as were plotted in Figure 7b. The dot-dashed curves in Figure 9 are found for plasmasphere (thick dot-dashed curve in Figure 9) and plasmatrough (thin dot-dashed curve in Figure 9) from the n_{e0} values plotted in Figure 7a in the following way: if $n_{e0} \geq 150$ cm^{-3}, $\alpha = 0$, while if $n_{e0} \leq 150$ cm^{-3}, n_e at $R = 2\ R_E$ is 150 cm^{-3}, and α is found from equation (3). It is clear that this simple model (dot-dashed curves in Figure 9) captures the general trend of the dependence of α with respect to R_{max}.

5. Kp Dependence

5.1. Dependence of α

[36] As discussed in section 1, *Denton et al.* [2002b] found that they could model α using equation (2) as a function of n_{e0} and R_{max}. Here we examine the α dependence as a function of MLT and the averaged Kp, $\langle$Kp$\rangle$. Following *Gallagher et al.* [1988], we calculate the average at the current time t by averaging over earlier times t' using the weighting factor $\exp(-(t - t')/t_0)$, where $t_0 = 3.0$ days. (*Denton et al.* [2002a] used 1.5 days, but we find that a 3-day timescale yields a parameter that correlates better to changes in density as described in sections 5.2 and 5.3.) Figure 10 indicates that there is no clear dependence of the average $\alpha - \alpha_{model}$ on MLT or $\langle$Kp$\rangle$. (The last $\langle$Kp$\rangle$ bin with $\langle$Kp$\rangle = 3.7$ shows $\alpha - \alpha_{model}$ slightly higher than 0, $\sim$0.5, but there are not many data points in this bin, and the scatter in $\alpha - \alpha_{model}$ at this value of $\langle$Kp$\rangle$ is very large.) Since there is a significant dependence of α on MLT and $\langle$Kp$\rangle$ (as shown by *Denton et al.* [2002a]), this indicates that the MLT and Kp α dependence can be accounted for predominantly by changes in n_{e0}.

5.2. Kp Dependence of n_e

[37] Figure 11 shows the $\langle$Kp$\rangle$ dependence of the electron density n_e at the magnetic equator (solid curves) and at $R = 2\ R_E$ (dashed curves). Figure 11a shows the $\langle$Kp$\rangle$ dependence for the plasmasphere data, while Figure 11b shows the $\langle$Kp$\rangle$ dependence for the plasmatrough data. The three

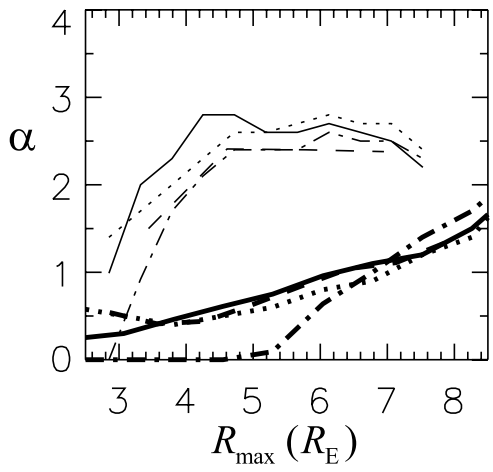

Figure 9. The thick and thin solid, dashed, and dotted curves are the same as were plotted in Figure 7b. The dot-dashed curves are found from the n_{e0} curves in Figure 7a (solid curves in Figure 7a) for plasmasphere (thick dot-dashed curve in this figure) and plasmatrough (thin dot-dashed curve in this figure) in the following way: if $n_{e0} \geq 150$ cm^{-3}, $\alpha = 0$, while if $n_{e0} \leq 150$ cm^{-3}, n_e at $R = 2\ R_E$ is 150 cm^{-3}, and α is found from equation (3).

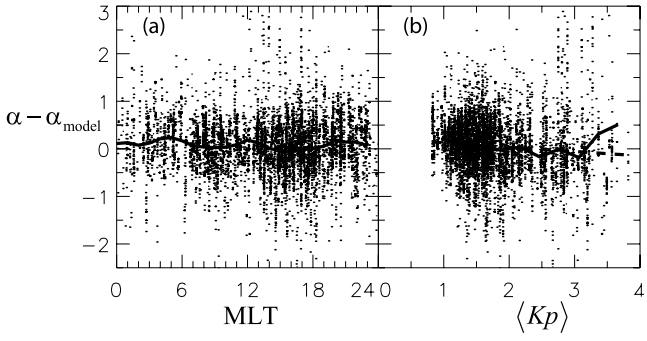

Figure 10. Plot of $\alpha - \alpha_{model}$ values versus (a) MLT and (b) ⟨Kp⟩ (average of Kp with a timescale of 3 days as described in section 5.1) for all categories of plasma data combined. The solid curves show the average values in bins (1 hour bins for MLT), while the dashed line in Figure 10b) is a linear fit.

curves for each type of data represent the log average value of the density (middle curve) and the log average plus or minus one standard deviation (upper and lower curves). Thus the three solid curves in Figure 11a show the log average value of the density versus ⟨Kp⟩ for the plasmasphere at $R = R_{max}$ (the magnetic equator) and the log average plus or minus one standard deviation. In order to reduce the effect of the R_{max} dependence, we have fit the n_e curves in Figure 7 with functions $n_{eL}(R_{max})$, and the density values have been divided by this function (evaluated at the R_{max} value corresponding to each data point) before binning the n_e/n_{eL} values with respect to ⟨Kp⟩. Thus the overall vertical position of each set of three n_e/n_{eL} curves in Figure 11 should be ignored. The important thing to note is the ⟨Kp⟩ dependence of each set of three curves and the relative spread of the three curves.

[38] Figure 11a shows that for the plasmasphere, the average density at the magnetic equator (middle solid curve) decreases significantly with respect to ⟨Kp⟩ (a factor of 2.0 between ⟨Kp⟩ = 1.1 and ⟨Kp⟩ = 3.3). This is to be expected if low ⟨Kp⟩ indicates that more refilling has been allowed to take place. The average density at $R = 2\ R_E$ (middle dashed curve) shows a smaller decrease in density with respect to ⟨Kp⟩. In the plasmatrough the average density at the magnetic equator (middle solid curve in Figure 11b) decreases a small amount with respect to ⟨Kp⟩ (24% between ⟨Kp⟩ = 1.3 and ⟨Kp⟩ = 3.5). The plasmatrough density at $R = 2\ R_E$ (middle dashed curve in Figure 11b) also decreases with respect to ⟨Kp⟩ for ⟨Kp⟩ < 2.5 but then appears to increase with respect to ⟨Kp⟩ at ⟨Kp⟩ > 2.5. Considering the large uncertainty and the fact that there are only six events represented in the two data bins with the largest values of ⟨Kp⟩, it would be unwarranted to stress this result too much. However, if further study verifies this dependence, the trend at low ⟨Kp⟩ could be caused by the same effect seen in the plasmasphere data, that at lower ⟨Kp⟩ there has been more refilling. At high ⟨Kp⟩, there might be no significant refilling (due to the large activity), and in that case, the larger density at high ⟨Kp⟩ could be due to greater ionospheric outflow at high Kp. A study of the polar region, where the magnetic field lines are open, shows that the electron density is higher at large Kp [*Nsumei et al.*, 2003]. (See section 3.1 for a discussion of the similarities between the plasmatrough and polar cap.)

[39] The smallest spread in the values (width between the upper and lower curves) occurs for the plasmatrough data values at $R = 2\ R_E$ (dashed curves in Figure 11b). This is understandable considering that the plasmatrough data best represents the levelling off of n_e at large R_{max} described in section 4.2, since the plasmatrough data more typically has a low value of n_e approaching ~100 cm^{-3}. (On the other hand, see the discussion in the last paragraph of section 4.2.)

[40] In addition to the ⟨Kp⟩ dependence shown in Figure 11, it is important to note that the plasmasphere data set has on average a lower value of ⟨Kp⟩ = 1.6 than does the plasmatrough data set, with ⟨Kp⟩ = 2.3. Noting the large difference in the n_{e0} values plotted in Figure 7a for the plasmasphere (thick solid curve in Figure 7a) and plasmatrough (thin solid curve in Figure 7a), the greatest effect of

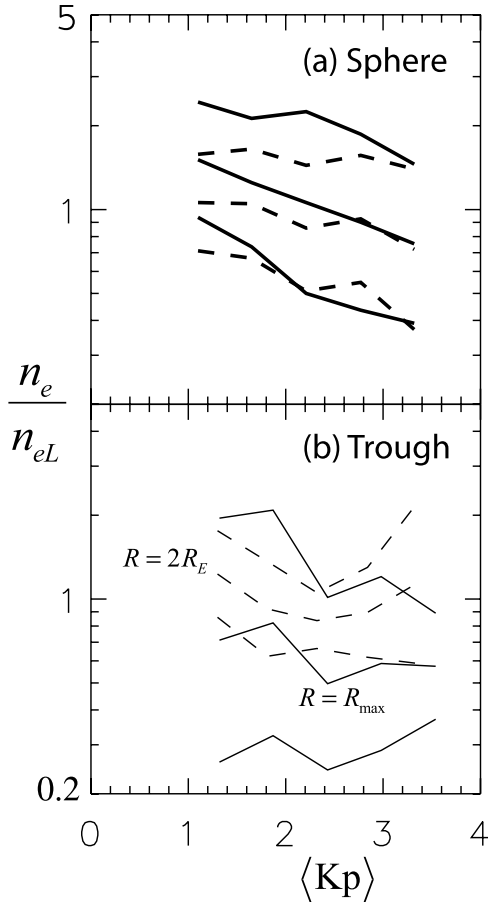

Figure 11. ⟨Kp⟩ dependence of the electron density n_e for (a) the plasmasphere and (b) plasmatrough. The values of n_e collected in ⟨Kp⟩ bins have been normalized to an L-dependent (or rather R_{max}-dependent) function as described in the text. The solid curves represent the ⟨Kp⟩ dependence for the density at $R = R_{max}$ (the magnetic equator), while the dashed curves give the ⟨Kp⟩ dependence for the density at $R = 2\ R_E$. The middle curve in each set of three (solid or dashed) is the log average density in the ⟨Kp⟩ bin, while the upper and lower curves are the log average plus or minus one standard deviation.

⟨Kp⟩ on the density is likely to be its effect on the type of plasma observed (sphere or trough).

5.3. Kp Dependence of n_e From CRRES Data

[41] While Figure 11 shows that the equatorial density decreases for increasing ⟨Kp⟩ (particularly for the plasmasphere), this result seems to be contradicted by the results of *Sheeley et al.* [2001], based on plasma wave measurements of electron density observed by the CRRES spacecraft. Figure 6 of their paper shows that the electron density does not depend on Kp_{max}, where Kp_{max} is the maximum value of Kp during the last 24 hours before each density measurement. Because of this difference in results, we have reanalyzed the CRRES data ourselves (see *Sheeley et al.* [2001] for a description of the data). Figures 12 and 13 show the results of our analysis for the plasmasphere and plasmatrough, respectively. Here, we follow Sheeley et al. and use equation (14) as the borderline density separating plasmasphere and plasmatrough data. (As discussed in section 4.1, this borderline value works fairly well for distinguishing the plasmasphere and plasmatrough data; the equation (15 cm^{-3}) $(6.6/\bar{R}_{max})^4$ does even better.) The dotted curves in Figure 12a show the log average electron density n_e versus Kp_{max} for the L-shell ranges indicated in the figure. These curves should be similar to the curves in Figure 6b of *Sheeley et al.* [2001]. However, unlike Sheeley et al., we find a clear trend of decreasing n_e with respect to Kp_{max}, especially at the lower L values. The solid curves in Figure 12a show the log average n_e versus ⟨Kp⟩ (averaged with a 3-day timescale; see section 5.1). It is clear that there is even a stronger dependence of n_e on ⟨Kp⟩ than on Kp_{max}, and therefore ⟨Kp⟩ is a better indicator of the Kp dependence. This is not surprising considering that ⟨Kp⟩ is a

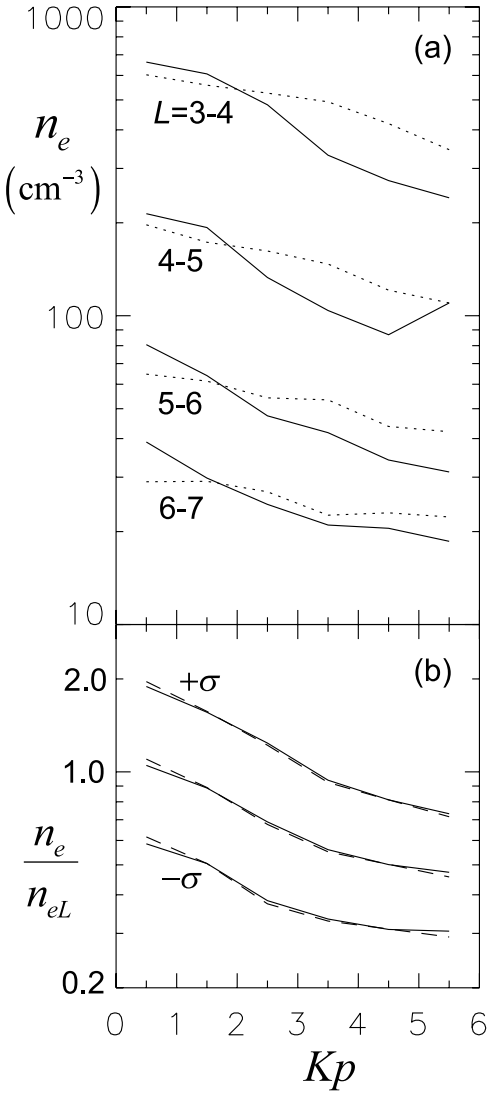

Figure 12. Electron density n_e versus Kp for the plasmasphere using the CRRES plasma wave data set [*Sheeley et al.*, 2001]. In Figure 12a the log average electron density n_e versus ⟨Kp⟩ (solid curves) and versus Kp_{max} (dotted curves) for the L shell ranges indicated in the figure. In Figure 12b the log average of values of n_e normalized to Sheeley et al.'s L-dependent plasmasphere model density (equation (8)) versus ⟨Kp⟩ (dashed curves). The middle dashed curve is the log average value in each ⟨Kp⟩ bin, while the upper and lower dashed curves are the log average plus or minus one standard deviation. The solid curves are the same as the dashed curves, except that the density values have been adjusted to equatorial values n_{e0} using equation (1) with equation (2).

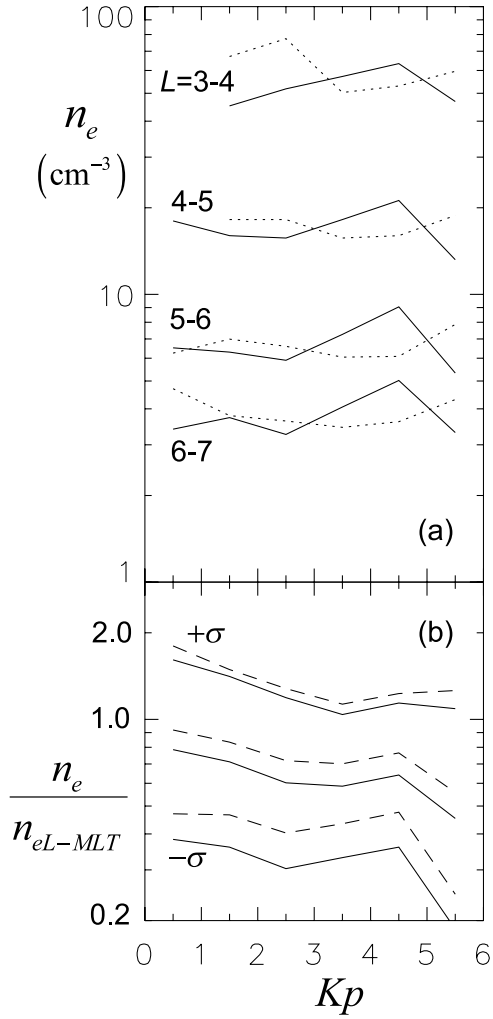

Figure 13. Like Figure 12, except for the plasmatrough data.

measure of the cumulative activity as opposed to the activity during one particular hour of time.

[42] The solid curves in Figure 12b are roughly equivalent to the solid curves in Figure 11. Here, the n_e values have been normalized to Sheeley et al.'s L-dependent plasmasphere model density (equation (8)), and the values of n_e/n_{eL} are plotted versus $\langle Kp \rangle$. Since CRRES did not have a polar orbit, we do not have paired measurements at one value of L with different radii (CRRES had an orbit inclined 18° from the geographic equator). Therefore in order to calculate the equatorial density, we have used equation (1) with equation (2). (In this subsection, the dipole field model is used.) The middle solid curve is the log average value of n_e/n_{eL}, while the upper and lower curves are the log average value plus or minus one standard deviation. The dashed curves are the same except that the measured n_e values are used with no correction to n_{e0}. In this case, the solid and dashed curves are almost indistinguishable. This is because at the high densities characteristic of the plasmasphere, α is small so that equation (1) leads to roughly constant density along the field line and the difference between the locally measured n_e and n_{e0} is small. (The unadjusted n_e values were also used in Figure 12a.) The decrease in n_e/n_{eL} with respect to $\langle Kp \rangle$ in Figure 12b is larger than the uncertainty, which helps us have some confidence that the Kp dependence for the plasmasphere density is real. Over the same range of $\langle Kp \rangle$ as was plotted in Figure 11 (1.1–3.3), n_e/n_{eL} decreases by a factor of 1.6, somewhat smaller than the decrease in Figure 11 (a factor of 2.0).

[43] Figure 13 shows the same quantities as were plotted in Figure 12, except for the CRRES plasmatrough data set (n_e values lower than the value of n_e given by equation (14)). From the dotted curves in Figure 13a, we can see that there is no apparent dependence of n_e versus Kp_{max}. Neither is the dependence of n_e on $\langle Kp \rangle$ very clear (solid curves in Figure 13a). On the other hand, when the density values are normalized to *Sheeley et al.*'s [2001] plasmatrough model including MLT dependence (their equation (7)),

$$n_{e0} = 124\ \mathrm{cm}^{-3}(3/\bar{R}_{max})^{4.0}, + 36\ \mathrm{cm}^{-3}(3/\bar{R}_{max})^{3.5}\cos\left(\left\{MLT - \left[7.7(3/R_{max})^{2.0}+12\right]\right\}\cdot\{\pi/12\}\right), \quad (16)$$

there is an apparent dependence of the normalized n_e/n_{eL-MLT} on $\langle Kp \rangle$ (Figure 13b; here n_{eL-MLT} is dependent on both L and MLT). The biggest factor causing n_e/n_{eL-MLT} to decrease with respect to $\langle Kp \rangle$ is the MLT dependence; if the MLT-dependent cosine term in equation (16) is neglected, n_e/n_{eL-MLT} does not decrease with respect to $\langle Kp \rangle$. The MLT dependence makes a difference in the results because the average Kp values were higher during the middle of 1991 when CRRES was sampling the afternoon MLT values than when it sampled dawn and nighttime MLT values. In fact, the average value of Kp was 2.2 during the first part of the CRRES mission, 1 August 1990 to 23 March 1991, but 3.2 from the 24 March 1991 storm to the end of the mission on 12 October 1991. CRRES did not completely sample all MLT values during its entire mission; the apogee of the orbit started in the dawn MLT sector and moved through midnight to afternoon MLT values at the end of the mission. The large density values at $\langle Kp \rangle \sim 4.5$ in Figure 13a are predominantly at afternoon values of MLT, where n_{eL-MLT} (equation (16)) has a peak with respect to MLT. (This correlation between Kp and MLT for the CRRES data will obviously complicate modeling both the Kp and MLT dependence.)

[44] As seen from Figure 13b, the total decrease in n_e/n_{eL-MLT} over the range of $\langle Kp \rangle$ plotted is a factor of 1.6 (as compared to 2.2 for the plasmasphere). Note also that for the plasmatrough data, the use of equation (1) with equation (2) to find n_{e0} makes a greater difference than it did for the plasmasphere, as indicated by the difference between the solid and dashed curves in Figure 13b. This is because the values of n_{e0} are lower for the trough, so α from equation (2) is larger.

[45] The plasmatrough density may be dependent on Kp as indicated by Figure 11b and Figure 13b, but considering the small amount of data at large Kp represented in Figure 11b and the lack of any Kp dependence in Figure 13a, we are hesitant to come to a firm conclusion about this dependence without further study. However, the dependence in the plasmasphere is more clear. We would most expect to see Kp dependence for the plasmasphere, since the plasmasphere develops from a period of refilling. Furthermore, the observed Kp dependence can account for the difference between the average plasmasphere model from our results (thick solid curve in Figure 6, which we have fit by equation (5) with equation (9)) and that of *Sheeley et al.* [2001] (thick dashed curve in Figure 6, found from equation (8)). The average value of $\langle Kp \rangle$ for CRRES's plasmasphere data (density measurements with n_e greater than the value of n_e given by equation (14)) is 2.5, whereas the average value for our Polar plasmasphere data set is 1.6. On the basis of Figure 11, this would cause the CRRES average density to be ~30% lower than the Polar average density, and this is about the difference between the two curves in Figure 6 (thick solid and thick dashed curves). If the average value of $\langle Kp \rangle$ is even lower for the plasmasphere data of *Carpenter and Anderson* [1992], the fact that their density is higher than the other models (at least for $R_{max} \geq 4\ R_e$; see Figure 6) could be accounted for.

6. Summary

[46] The Polar PWI data set spans the parameters $2.5\ R_e \leq R_{max} \leq 8.5\ R_e$, $2\ R_e \leq R \leq R_{max}$, and $2 \leq n_{e0} \leq 1500\ \mathrm{cm}^{-3}$, and this data set has been used to generate a model for the average α (equation (2)) as a function of equatorial density n_{e0} and R_{max} assuming the power law form for n_e (equation (1)) [*Denton et al.*, 2002b]. Variations of the average α with respect to MLT or Kp [*Denton et al.*, 2002a] can be attributed predominantly to changes in n_{e0} (Figure 10). Typical values of α were 0–1 in the plasmasphere and 2–3 in the plasmatrough (Figure 7b). While the low α values within the plasmasphere are consistent with diffusive equilibrium, the larger α values characteristic of the plasmatrough have a dependence which is intermediate between diffusive equilibrium and a collisionless model (roughly $n_e \propto R^{-4}$) [*Lemaire and Gringauz*, 1998]. It is important to note that our results describe only the average field line dependence; there will surely be deviations from the average behavior, some of which will be related to time-dependent effects.

[47] We have examined several events with electron density n_e measured on large and small radius portions of

an orbit (Figures 2–5). These events exhibit features that we commonly find in the Polar data. In particular, the plasmapause is much more evident on the part of the orbit with large radius (near the magnetic equator) than on the part of the orbit with small radius ($R = 2–3\ R_e$), and on the small radius portion of the orbit where $R \sim 2\ R_e$, n_e often levels off to $n_e \sim 100\ cm^{-3}$ at large R_{max}. This is consistent with the results of *Reinisch et al.* [2004] for plasmaspheric field lines, who show that temporal variations associated with flux tube depletion and refilling are less at low altitude than at the magnetic equator. We also present an example of plasmaspheric plasma extending out to at least $L \sim 9$ on the dawnside during particularly calm geomagnetic conditions (as indicated by Kp; see section 3.3).

[48] We have calculated the average equatorial profile of n_{e0} versus R_{max} for the plasmasphere data (including the "gradually decreasing" category of *Denton et al.* [2002a] (Appendix A) and find that it lies between the plasmasphere models of *Carpenter and Anderson* [1992] and *Sheeley et al.* [2001]. Our average plasmatrough density scales with respect to R_{max} like $\bar{R}_{max}^{-3.4}$. However, excluding the largest R_{max} values $\geq 6\ R_e$ (at which we have reason to doubt the accuracy of our average values; see section 4.1), our plasmatrough n_{e0} agrees well with *Sheeley et al.*'s [2001] result $\bar{R}_{max}^{-4.0}$ or with Carpenter and Anderson's $\bar{R}_{max}^{-4.5}$ (Figure 6).

[49] In addition to the average equatorial profile, we also calculated the log average n_e values at $R \sim 2\ R_e$ versus R_{max} (dashed curves in Figure 7a). Like the density profiles for the example events, these also level off at $\sim n_e \sim 100\ cm^{-3}$ at large R_{max}. We also found profiles of n_e at $R = 2\ R_e$ by using equation (2) with our average n_{e0} profiles as an input (dotted curves in Figure 7a). These also approached values of $n_e \sim 100–200\ cm^{-3}$ at large R_{max}. The same result was also observed in the meridional structure of our plasmatrough results (equation (12) with equation (2)), as shown in Figure 8. These properties are similar to those of the density in the polar cap, where the density is mostly a function of radius [*Nsumei et al.*, 2003]. However, the field line dependence and Kp dependence for the plasmatrough are not the same as in the polar cap (sections 3.3 and 5.3).

[50] There were some differences in the n_e values at $R \sim 2\ R_e$, depending on how they were calculated (log average values or the value found using equation (2) with n_{e0} as an input). Correspondingly, there were also differences in the α values computed in different ways (average value, value from equation (2), or value found using equation (3) with the average n_{e0} and value of n_e for $R = 2\ R_e$; these are plotted in Figure 7b). These differences demonstrate the limitations of our power law model.

[51] We need to keep in mind the fact that some low-density measurements at low radius could be missed because $f_p/f_{ce} < 1$ (section 3.4). This could bias our results somewhat. In particular, the density at low radius and large R_{max} might have in some cases decreased significantly below $100\ cm^{-3}$, and PWI could not measure it. On the other hand, we often see the density level off at $n_e \sim 100\ cm^{-3}$ at small radius and large R_{max} when the equatorial density is still decreasing with respect to R_{max} (Figures 2a and 5a), and $n_e \sim 100\ cm^{-3}$ at $R \sim 2\ R_e$ is consistent with the average field line dependence using density measurements at higher altitude (Figure 7 and discussion in the last paragraph of section 4.2).

[52] We also presented a simplified model for α using the observations that at large equatorial density n_{e0}, the density is roughly constant along field lines and that n_e at $R \sim 2\ R_e$ approaches as a rough lower limit $100\ cm^{-3}$. This simple model (dot-dashed curves in Figure 9) captures the general trend of the dependence of α with respect to R_{max}, though the agreement with the other values of α is certainly not exact.

[53] Finally, we examined the Kp dependence of the equatorial density and density at $R \sim 2\ R_e$. For the equatorial density, we supplemented our Polar data set with data from the CRRES spacecraft [*Sheeley et al.*, 2001]. The plasmasphere n_e values at the magnetic equator clearly decrease with respect to $\langle Kp \rangle$ (Kp averaged with a 3-day timescale as described in section 5.1), as shown in Figures 11a and 12. We also showed that the quantity $\langle Kp \rangle$ better indicates the variation of density with respect to Kp than the maximum value of Kp during the last 24 hours (section 5.3). The fact that the plasmasphere density decreases with respect to $\langle Kp \rangle$ is consistent with the idea that greater refilling occurs over a period of low geomagnetic activity. This dependence of the plasmasphere density on $\langle Kp \rangle$ can also explain the difference in the average density based on the Polar data and that of Sheeley et al., as shown in the last paragraph of section 5.3. The dependence of the plasmatrough density with respect to $\langle Kp \rangle$ is not so clear and perhaps more complicated.

Appendix A: Definitions of Plasmasphere and Plasmatrough Data

[54] *Denton et al.* [2002b] separated the Polar PWI data into three categories. If there was a plasmapause (drop in n_e of at least a factor of 3 within $\Delta R_{max} = 0.4$), they categorized the density data inside (outside) the plasmapause as plasmasphere (plasmatrough) data. If the orbit had only n_e values $>300\ cm^{-3}$, they categorized it as plasmasphere data. The plasmatrough data was almost exclusively identified as the region outside a plasmapause; however, in some cases no plasmapause was discernable, but the density was so low that the data was categorized as plasmatrough data. For instance, in one case, n_e was $\sim 30\ cm^{-3}$ at $R_{max} \sim 4\ R_e$ and decreased gradually down to values $\sim 10\ cm^{-3}$ at larger R_{max}. Sometimes n_e decreased gradually with respect to R_{max} from values $>300\ cm^{-3}$ to values $\sim 10\ cm^{-3}$ with no clear plasmapause (Figure 5), and they counted this data as a third "gradually decreasing" (no plasmapause) category. In most cases in the gradually decreasing category, the density at low R_{max} was higher than $300\ cm^{-3}$, $\sim 1000\ cm^{-3}$ at $R_{max} \sim 3\ R_e$ and $\sim 500\ cm^{-3}$ at $R_{max} \sim 3\ R_e$. For the purposes of this paper, the plasmasphere and "gradually decreasing" categories are combined into a new plasmasphere category. The "gradually decreasing" plasma is assumed to be extended plasmasphere.

Appendix B: Details Concerning Figure 5

[55] Profiles of density with respect to R_{max} similar to that shown in Figure 5 were observed at the same MLT $\sim$ 7–8 hours on the next two Polar passes, on 20 December 1996 at 1615–1826 UT and on 21 December at 0950–1210 UT. Similar profiles of density versus R_{max} were also observed at dusk MLT $\sim$ 20 hours, before and after the time corresponding to the event in Figure 5 (at 19 December,

0747–1010 UT, and at 20 December, 0100–0310 UT, 20 December, 1853–2045 UT, and 21 December, 1248–1435 UT). The 20 December, 0100–0310 UT observation included "gradually decreasing" density out to at least $R_{max} \sim 12\ R_e$. On the other hand, a plasmapause at $R_{max} = 5\ R_e$ with a drop in density of a factor of 5 was observed at MLT $\sim$ 0800 (same MLT as Figure 5) at 17 hours (UT) earlier than the time corresponding to Figure 5. In order to interpret the "gradually decreasing" condition (no plasmapause) as applying uniformly to all azimuths, it is necessary to assume that the density increased significantly in the region just outside $R_{max} = 5\ R_e$ from $\sim$20 cm^{-3} to $\sim$200 cm^{-3} during a period of 17 hours. The existence of this extended plasmasphere density correlated with an extended period of low geomagnetic activity as indicated by a low value of Kp. Data from NSSDC OMNIWeb (NOAA) shows that the hourly average Kp on 19 December 1996 was equal to 0.7 from 0000 to 0200 UT, 0 from 0300 to 2000 UT, 0.7 from 2100 to 2300 UT, and 0 again at 2400 UT. At 2300 UT, the value of Kp averaged using the technique of section 5.1 (with a timescale of 3.0 days), $\langle Kp \rangle$, was 1.0.

Appendix C: Total Flux Tube Particle Content

[56] The total flux tube particle content (per flux) will be constant across the plasmatrough under the assumptions that (1) the plasmatrough flux tubes are simultaneously depleted at some time, (2) they subsequently begin to refill due to upward flux of particles from the ionosphere, (3) a similar fraction of that upward flux is trapped in each flux tube, and (4) the plasmatrough flux tubes map down to a similar latitude at the Earth's surface. The last condition results from the geometry of the nearly dipolar magnetic field. Because the flux tubes map down to a similar latitude at the Earth's surface, B at the Earth's surface is roughly constant with respect to L so that the area of a flux tube (per magnetic flux) at the Earth's surface is roughly constant. The other consequence of the flux tubes mapping to a similar latitude is that the upward refilling flux of particles (particles per area per time) from the ionosphere will be roughly constant with respect to L. Then the particles per time filling the flux tube will be constant with respect to L.

[57] **Acknowledgments.** We are grateful to Iowa PWI team, including D. Gurnett and J. Pickett, for supplying the upper hybrid resonance data (supported by NASA grant NAG5-11942), the Polar spacecraft science data team for supplying spacecraft ephemeris data, and NSSDC for making the IMP-8 (GSFC and LANL) and WIND (courtesy of R. P. Lepping and K. W. Ogilvie) solar wind data, Dst (Kyoto University), and Kp (NOAA) data available on OMNIWeb. We thank Mark Moldwin for useful discussions relating to the CRRES data. Work at Dartmouth was supported by NSF grant ATM-0245664. Work at the University of Iowa was supported by NASA grants NAG5-11942 and NAG5-9561.

[58] Arthur Richmond thanks Dennis Gallagher and another reviewer for their assistance in evaluating this paper.

References

Carpenter, D. L., and R. R. Anderson (1992), An ISEE/whistler model of equatorial electron density in the magnetosphere, *J. Geophys. Res.*, *97*, 1097.

Denton, R. E., E. G. Miftakhova, M. R. Lessard, R. Anderson, and J. W. Hughes (2001), Determining the mass density along magnetic field lines from toroidal eigenfrequencies: Polynomial expansion applied to CRRES data, *J. Geophys. Res.*, *106*, 29,915–29,924.

Denton, R. E., J. Goldstein, J. D. Menietti, and S. L. Young (2002a), Magnetospheric electron density model inferred from Polar plasma wave data, *J. Geophys. Res.*, *107*(A11), 1386, doi:10.1029/2001JA009136.

Denton, R. E., J. Goldstein, and J. D. Menietti (2002b), Field line dependence of magnetospheric electron density, *Geophys. Res. Lett.*, *29*(24), 2205, doi:10.1029/2002GL015963.

Denton, R. E., K. Takahashi, R. R. Anderson, and M. P. Wuest (2004), Magnetospheric toroidal Alfven wave harmonics and the field line distribution of mass density, *J. Geophys. Res.*, *109*, A06202, doi:10.1029/2003JA010201.

Gallagher, D. L., P. D. Craven, and R. H. Comfort (1988), An empirical model of the Earth's plasmasphere, *Adv. Space Res.*, *8*, 15.

Gallagher, D. L., P. D. Craven, and R. H. Comfort (2000), Global core plasma model, *J. Geophys. Res.*, *105*, 18,819.

Goldstein, J., R. E. Denton, M. K. Hudson, E. G. Miftakhova, S. L. Young, J. D. Menietti, and D. L. Gallagher (2001), Latitudinal density dependence of magnetic field lines inferred from Polar plasma wave data, *J. Geophys. Res.*, *106*, 6195.

Gurnett, D. A., and U. S. Inan (1988), Plasma wave observations with the Dynamics Explorer 1 spacecraft, *Rev. Geophys.*, *26*(2), 285–316.

Gurnett, D. A., et al. (1995), The Polar Plasma Wave Instrument, *Space Sci. Rev.*, *71*, 583.

Huang, X., B. W. Reinisch, P. Song, J. L. Green, and D. L. Gallagher (2004), Developing an empirical density model of the plasmasphere using IMAGE/RPI observations, *Adv. Space Res.*, *33*, 829–832.

IAGA Division V Working Group 8 (1991), International geophysical reference field, *J. Geomagn. Geoelectr.*, *43*, 1007.

Lemaire, J. F., and K. I. Gringauz (1998), *The Earth's Plasmasphere*, pp. 222–249, Cambridge Univ. Press, New York.

Lin, C. S., J. L. Burch, S. D. Shawhan, and D. A. Gurnett (1984), Correlation of auroral hiss and upward electron beams near the polar cusp, *J. Geophys. Res.*, *89*, 925–936.

Menk, F. W., D. Orr, M. A. Clilverd, A. J. Smith, C. L. Waters, D. K. Milling, and B. J. Fraser (1999), Monitoring spatial and temporal variations in the dayside plasmasphere using geomagnetic field line resonances, *J. Geophys. Res.*, *104*, 19,955.

Nsumei, P. A., X. Huang, B. W. Reinisch, P. Song, V. M. Vasyliunas, J. L. Green, S. F. Fung, R. F. Benson, and D. L. Gallagher (2003), Electron density distribution over the northern polar region deduced from IMAGE/radio plasma imager sounding, *J. Geophys. Res.*, *108*(A2), 1078, doi:10.1029/2002JA009616.

Persoon, A. M., D. A. Gurnett, and S. D. Shawhan (1983), Polar cap electron densities from DE-1 plasma wave observations, *J. Geophys. Res.*, *88*(A12), 123–136.

Reinisch, B. W., X. Huang, P. Song, G. S. Sales, S. F. Fung, J. L. Green, D. L. Gallagher, and V. M. Vasyliunas (2001), Plasma density distribution along the magnetospheric field: RPI observations from IMAGE, *Geophys. Res. Lett.*, *28*, 4521.

Reinisch, B. W., X. Huang, P. Song, J. L. Green, S. F. Fung, V. M. Vasyliunas, D. L. Gallagher, and B. R. Sandel (2004), Plasmaspheric mass loss and refilling as a result of a magnetic storm, *J. Geophys. Res.*, *109*, A01202, doi:10.1029/2003JA009948.

Sandel, B. R., R. A. King, W. T. Forrester, D. L. Gallager, A. L. Broadfoot, and C. C. Curtis (2001), Initial results from the IMAGE extreme ultraviolet imager, *Geophys. Res. Lett.*, *28*, 1439.

Sheeley, B. W., M. B. Moldwin, H. K. Rassoul, and R. R. Anderson (2001), An empirical plasmasphere and trough density model: CRRES observations, *J. Geophys. Res.*, *106*(A11), 25,631–25,641.

Takahashi, K., R. E. Denton, R. R. Anderson, and W. J. Hughes (2004), Frequencies of the standing Alfvén wave harmonics and their implication for plasma mass distribution along geomagnetic field lines: Statistical analysis of CRRES data, *J. Geophys. Res.*, *109*, A08202, doi:10.1029/2003JA010345.

Tataronis, J. A., and F. W. Crawford (1970), Cyclotron harmonic wave propagation and instabilities, I. Perpendicular propagation, *Plasma Phys.*, *4*, 231.

Tsyganenko, N. A. (1989), A magnetospheric magnetic field model with a warped tail current sheet, *Planet. Space Sci.*, *37*, 5.

Tsyganenko, N. A. (1995), Modeling the Earth's magnetospheric magnetic-field confined within a realistic magnetopause, *J. Geophys. Res.*, *100*, 5599.

R. R. Anderson and J. D. Menietti, Department of Physics and Astronomy, University of Iowa, Iowa City, IA 52242, USA. (rra@space.physics.uiowa.edu; jdm@space.physics.uiowa.edu)

R. E. Denton, Department of Physics and Astronomy, Dartmouth College, 6127 Wilder Laboratory, Hanover, NH 03755, USA. (richard.e.denton@dartmouth.edu)

J. Goldstein, Southwest Research Institute, P.O. Drawer 28510, San Antonio, TX 78228-0510, USA. (jerry.goldstein.adv00@alum.dartmouth.org)

S. L. Young, AFRL/VSBXR, 29 Randolph Road, Hanscom AFB, MA 01731-3010, USA. (shawn.young@hanscom.af.mil)